ACS OMEGA

Open Access

http://pubs.acs.org/journal/acsodf

Article

Multilayer Carbon Nanotube Film/*Eucommia ulmoides* Gum Composite Films with Excellent Electromagnetic Shielding Performance and Infrared-Triggered Shape Memory Behavior

Zhonglei Kang and Bo-xing Zhang*

Cite This: *ACS Omega* 2024, 9, 48563−48570

Read Online

ACCESS | Metrics & More | Article Recommendations

ABSTRACT: Due to the increasing pressure of environmental protection and the depletion of oil resources, *Eucommia ulmoides* gum (EUG) as a natural renewable and degradable biopolymer has attracted more and more attention. In this work, multilayer carbon nanotube film (CNF)/EUG composite films were fabricated through the infiltration and hot-pressing process. By taking advantage of the elasticity of EUG and the specific strength of CNF, composite films exhibited much more improved mechanical strength (maximum tensile stress up to 108.4 MPa) compared with pristine EUG and CNF alone. In addition, composite films prepared with five CNF layers and five infiltration cycles of EUG solution with a thickness of 181 μm can achieve the highest total shielding effectiveness value of 88 dB in 15.6 GHz. Moreover, the folded composite film can recover quickly to the fixed permanent shape when exposed to infrared light, demonstrating fascinating infrared-triggered shape memory behavior. This work provides a facile and general method to fabricate CNF/EUG composite films and is beneficial for pushing forward the practical application of EUG materials.

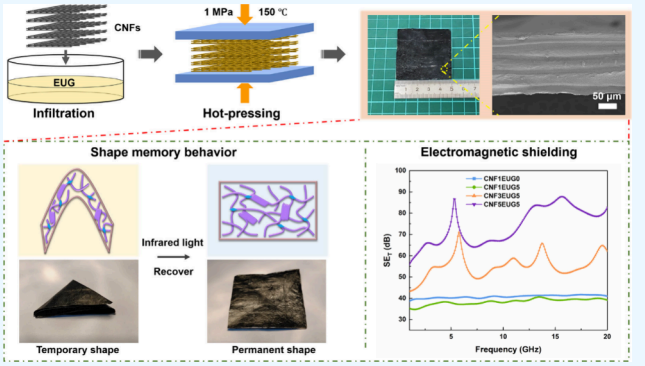

1. INTRODUCTION

Eucommia ulmoides gum (EUG) is an important biobased natural polymer with the chemical structure of trans-1, 4-polyisoprene, which is a renewable and degradable biopolymer material. Different from natural rubber, EUG possesses a unique duality of both rubber and plastic due to its higher crystallization.[1,2] In recent years, researches on EUG have mainly focused on modification including physical modification and chemical modification,[3−6] aiming to disrupt the orderliness of the molecular chain, reduce the crystallinity of EUG, and introduce some functional sites (hydroxyl, epoxy, disulfide, etc.). On this basis, various elastomers, self-healing materials, electromagnetic shielding materials, and shape memory materials were prepared successfully.[7−13]

Shape memory polymers (SMPs), which typically include a fixed phase and a reversible phase, are a new type of smart materials that enable them to recover their permanent shapes from temporary shapes in response to external stimuli.[14−16] Due to the coexistence of crystalline regions and cross-linked networks, partially cross-linked EUG has attracted considerable attention for applications in shape memory materials. To date, thermal-,[17−22] electro-,[23,24] and water-triggered[21] EUG-based shape memory materials have been prepared. Qi et al. synthesized body temperature-responsive EUG-based SMPs by varying the amount of hydrogen peroxide, which exhibits excellent shape memory ability with a shape fixity ratio of 99% and a recovery ratio near 100%.[17]

Two-dimensional carbon electromagnetic shielding composite films have been increasingly developed because of their light weight, high electrical conductivity, easy processing, flexibility, and excellent corrosion resistance. Early studies focused on producing monolayer materials by dispersing carbon materials (graphene, graphite, carbon nanotubes, carbon fibers, etc.) into polymer matrices to enhance electrical conductivity and electromagnetic shielding performance.[12,25−32] Compared to monolayer materials, multilayer materials display more structure designability and improved electromagnetic shielding performance.[33−40] Song et al.[33] proposed a novel multilayer electromagnetic shielding material prepared through the permutation and combination of graphene oxide films, graphene nanosheets, and electrical and magnetic loss spacers. The results show that sandwich structures were able to present unique frequency selectivity

Received: August 13, 2024
Revised: November 10, 2024
Accepted: November 19, 2024
Published: November 25, 2024

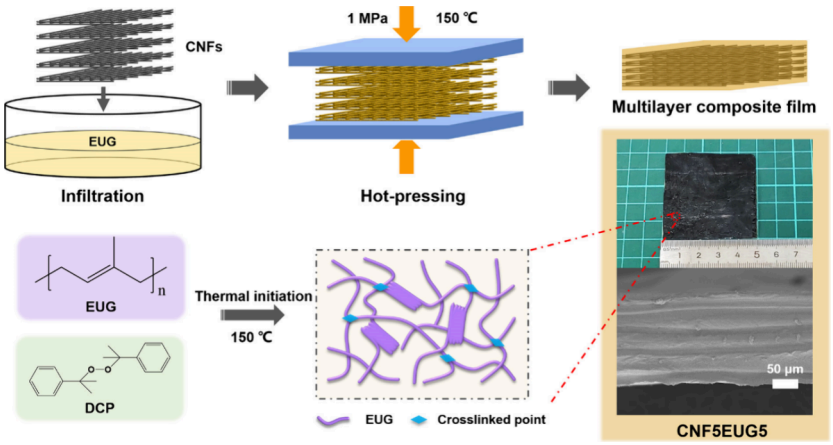

Figure 1. Schematic diagram of the preparation process for CNFaEUGb composite films.

and higher electromagnetic shielding performance due to the appearance of resonance features. Lin et al.[34] fabricated sandwich multilayer composites through a hot-pressing process combining the PP/MWCNT layer, the PVA/MWCNT layer, and the PVA/graphene nanosheet layer. The sandwich-structured composites have a desirable electromagnetic shielding performance in the frequency range of 1−2 GHz. In addition, the incorporation of maleic anhydride grafted polypropylene provides the composites with a higher tensile strength.

In some complex application conditions, electromagnetic interference (EMI) shielding materials are required to have tunable shielding effectiveness. Polyurethane/graphene composite foams with a porous microstructure exhibited tunable shielding performance through physical compression or release.[41] However, this adjustability must be assisted by external forces during the deformation process. Incorporating shape memory ability is considered a feasible strategy to realize tunable electromagnetic shielding properties without external forces. The shape memory effect enables stimuli-responsive shape switching between the original and temporary states, which is expected to trigger the modulation of shielding performance via spontaneous structure change.[42] MF@MA/PEG composites with shape memory properties realized the change of thickness under heating or light, exhibiting the possibility of adjusting EMI shielding performance.[43]

Carbon nanotube film (CNF) is a homogeneous two-dimensional network structure film consisting of disordered carbon nanotubes with a large aspect ratio. As revealed, carbon nanotubes have excellent electrical, thermal, mechanical, and electromagnetic shielding performance.[26,38,44] Therefore, the combination of CNF and partially cross-linked EUG is an appreciable strategy for the fabrication of lightweight, shape memory, and high-strength EUG-based electromagnetic shielding composite films, in which CNF plays an important role as the reinforcement and electromagnetic shielding agent.

In this work, we fabricated multilayer CNF/EUG composite films with infiltration and hot-pressing technologies. The influences of infiltration cycles and the number of CNF layers on the mechanical and electromagnetic shielding performances were systematically investigated. This work aims to develop functional EUG-based composite films with great mechanical properties, electromagnetic shielding performance, and shape memory capability.

2. EXPERIMENTAL SECTION

2.1. Materials. EUG ($M_w \approx 1.8 \times 10^5$ g/mol) was kindly offered by Xiangxi Laodie Biotechnology Co., Ltd., Jishou, China. Chloroform was purchased from the Guangzhou Chemical Reagent Factory, Guangzhou, China. Dicumyl peroxide (DCP) was obtained from Shanghai Aladdin Biochemical Technology Co., Ltd., Shanghai, China. CNFs (thickness 10−20 μm, fiber diameter about 57 nm, and electrical conductivity $\approx 0.8 \times 10^5$ S/m) were supplied by Tanrand New Materials Technology Co., Ltd., Beijing, China. All reagents without special mention were used as received.

2.2. Preparation of Multilayer CNF/EUG Composite Films. EUG (1 g) and DCP (0.02 g) were dissolved completely in chloroform (99 g) at room temperature by stirring gently to obtain the 1 wt % EUG solution. Pristine CNF (50 × 50 mm) was dipped into the EUG solution for 10 min and dried at 50 °C for 5 min to remove the chloroform. This infiltration cycle was repeated for desired times of 1, 3, 5, and 7 to obtain the CNF/EUG prepregs (Figure 1). Higher concentrations (>1 wt %) of the EUG solution resulted in very high viscosities that were detrimental to the infiltration process, and lower concentrations (<1 wt %) necessitated more infiltration cycles to achieve the designed ratios of EUG and CNF. The resultant prepregs were laminated in a customized metal mold and hot-pressed with a temperature of 150 °C and a pressure of 1 MPa for 30 min. The final composite films were termed CNFaEUGb, where a is the number of CNF layers and b is the infiltration cycles. For example, CNF3EUG5 represents the composite films that are prepared with 3 layers of CNF and 5 filtration cycles.

2.3. Characterization. The morphology of multilayer composite films was imaged with a scanning electron microscope (SEM, JSM-7900F, JEOL, Japan) at 5 kV. Electromagnetic shielding performance was measured by a vector network analyzer (3656D, Ceyear Technologies Co., Ltd., China) using the flange coaxial test method in the frequency range of 1−20 GHz. The tensile tests were performed by universal testing machines (AG-IC50KN, SHIMADZU, Japan) at a crosshead speed of 1 mm/min to measure the tensile strength and elongation-at-break of the samples. Dumbbell-shaped samples were prepared with a custom cutter with a length of 50 mm and a width of 4 mm. For each sample, five replicates were tested, and the average values with standard deviations (SDs) were determined.

https://doi.org/10.1021/acsomega.4c07453
ACS Omega 2024, 9, 48563−48570

3. RESULTS AND DISCUSSION

3.1. Mechanical Properties and Microstructure of Composite Films. The combination of the infiltration and hot-pressing process facilitates the formation of cross-linked EUG structures and the strong adhesion between CNF and EUG, which can efficiently improve the mechanical properties of CNFaEUGb composite films. The tensile stress−strain curves of composite films with different infiltration cycles are shown in Figure 2A. CNF1EUG0 has a maximum tensile stress of 64.6 MPa and elongation-at-break of 21.1%. As the infiltration cycles increase, the CNF mass ratio (M_{CNF}) in composite films continues to decrease (Table 1), and the elongation-at-break of CNFaEUGb displays a steady increase and reaches the maximum value of 59.7% in CNF1EUG7. However, the maximum tensile stress of CNFaEUGb has a different tendency. The highest tensile stress achieved by CNF1EUG5 is 71.8 MPa, with an increase of 11.1% with respect to that of CNF1EUG0. Inversely, CNF1EUG7 has a lower maximum tensile stress of 58.64 MPa because the mechanical strength of EUG is inferior to that of CNF, and excess EUG will weaken composite films.

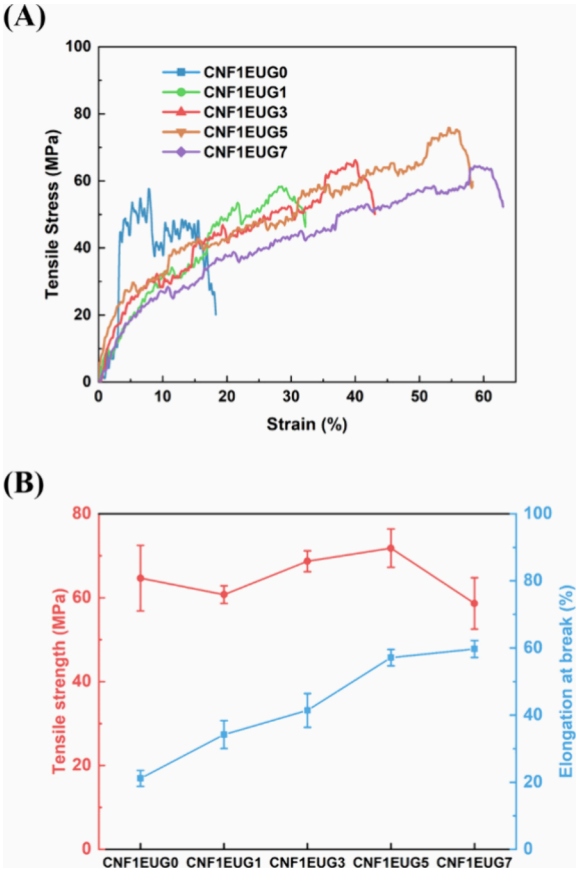

Figure 2. (A) Typical tensile stress−strain curves and (B) variation in mechanical properties of CNF1EUG0, CNF1EUG1, CNF1EUG3, CNF1EUG5, and CNF1EUG7.

Therefore, the infiltration cycle is optimized as five cycles because it can lead to maximum tensile strength and moderate elongation-at-break.

To investigate the effect of the number of CNF layers on the microstructure and mechanical properties of composite films, infiltration cycles were fixed at 5, and the number of CNF layers varied from 1 to 5 (CNF1EUG5, CNF3EUG5, and CNF5EUG5). Figure 3 shows the cross sections of these samples obtained by cutting with a blade. CNF1EUG0 has a loose porous structure comprising the stacking carbon nanotube. In contrast, CNF1EUG5, CNF3EUG5, and CNF5EUG5 have dense structures, attributed to the infiltration of EUG into CNF. Moreover, CNF layers and EUG were closely bonded without gaps and cracks, revealing the good compatibility between CNF and EUG, as well as the excellent adhesive properties of EUG.

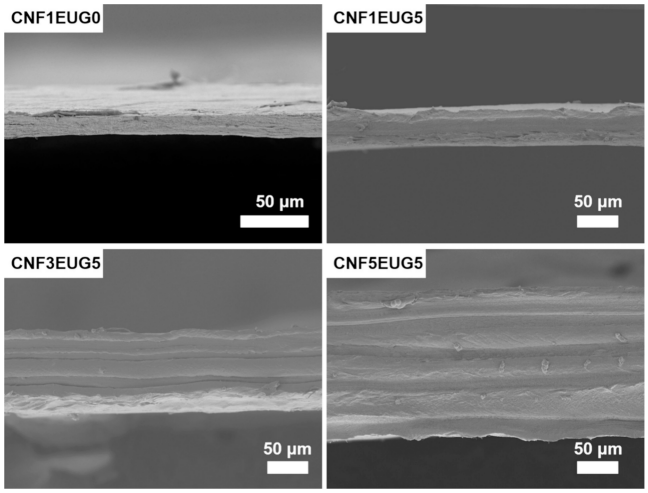

Figure 3. SEM images of the blade-cut cross sections of CNF1EUG0, CNF1EUG5, CNF3EUG5, and CNF5EUG5.

The tensile stress−strain curves of CNF1EUG5, CNF3EUG5, and CNF5EUG5 are shown in Figure 4. Three specimens exhibit an almost-linear range at low strain (<3%), followed by a hardening region, which continues up to 57.1% for CNF1EUG5, to 57.9% for CNF3EUG5, and to 61.5% for CNF5EUG5. It is noticed that there is no evident yielding plateau in the tensile stress−strain curves of CNF1EUG5,

Table 1. Denotation and Characteristics of the CNFaEUGb Composite Films[a]

samples	M_{CNF} (wt %)	thickness (μm)	maximum stress (MPa)	elongation-at-break (%)	maximum load (N)
CNF1EUG0	100	13.67	64.65 ± 7.84	21.14 ± 2.38	3.54 ± 0.52
CNF1EUG1	53.3	20.36	60.74 ± 2.08	34.20 ± 4.14	4.95 ± 0.21
CNF1EUG3	27.0	31.20	68.69 ± 2.50	41.41 ± 5.02	8.57 ± 0.38
CNF1EUG5	17.5	42.13	71.80 ± 4.56	57.14 ± 2.42	12.10 ± 0.94
CNF1EUG7	11.4	62.16	58.64 ± 6.11	59.70 ± 2.50	14.58 ± 1.86
CNF3EUG5	15.4	80.19	108.46 ± 8.10	57.93 ± 3.83	34.88 ± 3.09
CNF5EUG5	16.3	180.93	92.61 ± 4.28	61.54 ± 1.79	67.02 ± 3.80

[a] M_{CNF} is the ratio of the mass of CNF to the mass of composite films.

https://doi.org/10.1021/acsomega.4c07453
ACS Omega 2024, 9, 48563−48570

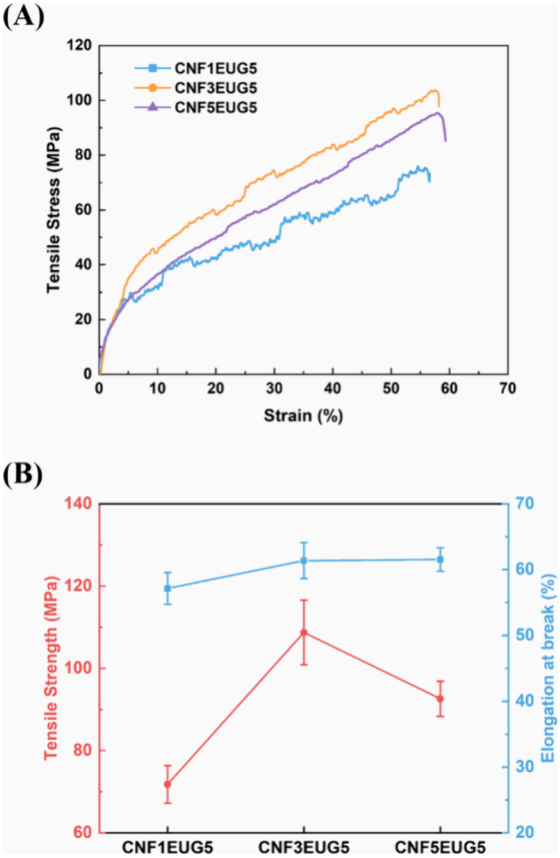

Figure 4. (A) Typical tensile stress−strain curves and (B) variation in mechanical properties of CNF1EUG5, CNF3EUG5, and CNF5EUG5.

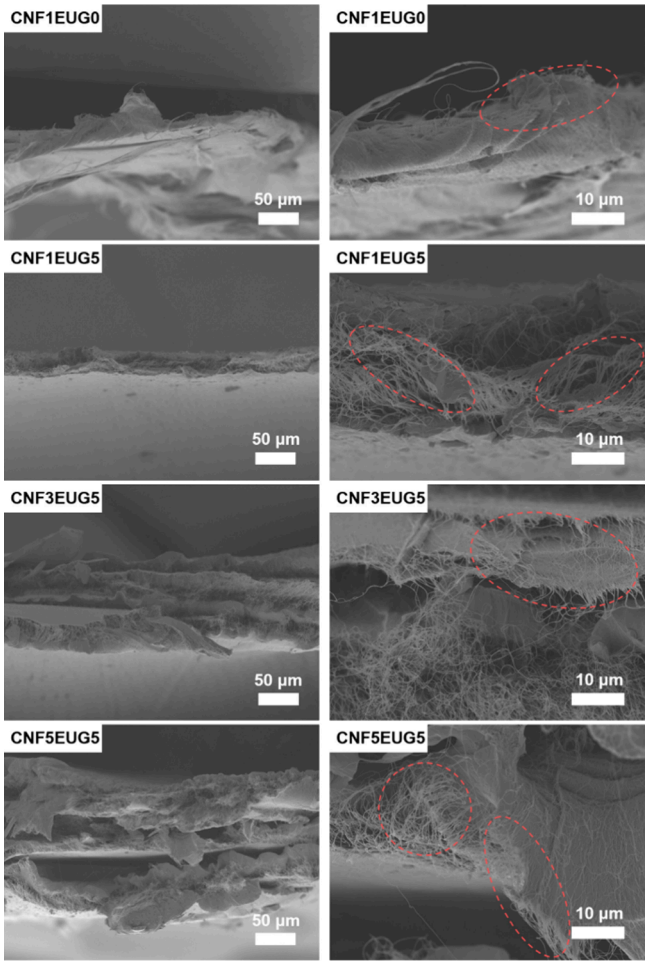

Figure 5. SEM images of the tensile fractured cross sections of CNF1EUG0, CNF1EUG5, CNF3EUG5, and CNF5EUG5 after the tensile tests.

CNF3EUG5, and CNF5EUG5 in comparison with EUG materials. The highest tensile stress achieved by CNF3EUG5 is 108.5 MPa with an increase of 51.1% in comparison to CNF1EUG5 (Table 1). In addition, CNF3EUG5 and CNF5EUG5 exhibit much uniform and steady load-bearing properties in comparison to CNF1EUG5, ascribed to the multilayer structure and the excellent CNF/EUG interfacial compatibility.

The tensile fractured morphology of the composite films was studied to elucidate the failure mode of the composite films. Figure 5 shows that samples have a rough irregular cross section and exhibit a typical ductile fracture behavior. During tensile testing, single-layer and multilayer composite films show different breakdown processes. Under the action of traction, CNF1EUG0 and CNF1EUG5 show a continuous cross-sectional reduction, followed by the necking phenomenon before complete failure. However, for CNF3EUG5 and CNF5EUG5, the fracture is initiated from the CNF located regions and gradually propagates to the CNF/EUG interfaces until breakdown, during which there is no necking phenomenon. It can be observed at the CNF/EUG interfaces that carbon nanotubes are elongated along the stretching direction (Figure 5). Due to the good adhesion of the CNF and EUG matrix, the matrix can effectively transmit stress to carbon nanotubes, and carbon nanotubes will be oriented under the stretching force until complete fracture. In addition, due to the low elongation of CNF, the breakdown of CNF is earlier than that of EUG, which is consistent with observations.

In summary, CNF/EUG composite films balance well the elasticity of EUG and the specific strength of CNF, together with the multilayer toughening mechanism, to achieve a mechanical performance much better than that of CNF and EUG alone.

3.2. Electromagnetic Shielding Performance. The electromagnetic shielding performance of CNFaEUGb with different layers of CNF is evaluated (Figure 6). CNF1EUG0 and CNF1EUG5 exhibit approximate total shielding effectiveness (SE_T) values of 40 and 38 dB, respectively, and no significant change in the 1−20 GHz range. Different from CNF1EUG0 and CNF1EUG5, the multilayer composite films CNF3EUG5 and CNF5EUG5 have better shielding performance with SE_T values of more than 43 and 55 dB in the whole testing band, respectively. In addition, CNF3EUG5 and CNF5EUG5 composite films show clear resonance-like features with peak SE_T values of 70 dB in 5.4 GHz, 58 dB in 11.4 GHz, and 67 dB in 18.3 GHz for CNF3EUG5 and 86 dB in 5.3 GHz, 83 dB in 13.1 GHz, and 88 dB in 15.6 GHz for CNF5EUG5.

CNF1EUG0 possesses electromagnetic shielding performance due to the formation of the conductive network that comprises stacking carbon nanotubes. For multilayer CNFaEUGb composite films, the EUG matrix is nearly electromagnetic wave transparent, and the electromagnetic shielding properties mainly come from CNF. The shielding

https://doi.org/10.1021/acsomega.4c07453
ACS Omega 2024, 9, 48563−48570

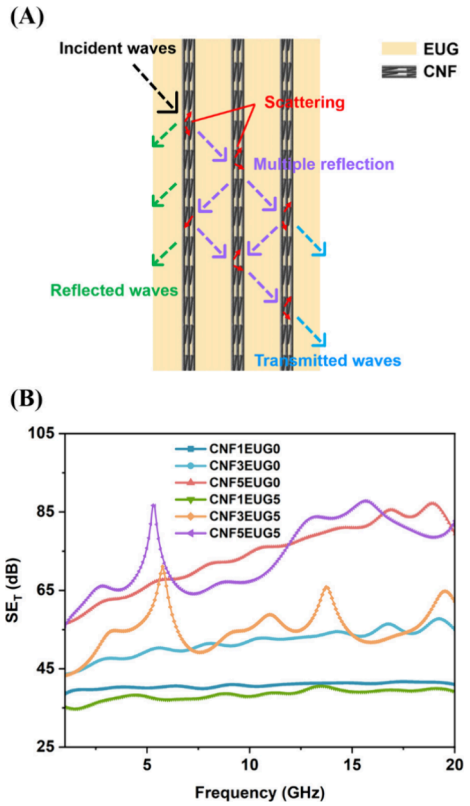

Figure 6. (A) Schematic representation of incident electromagnetic wave attenuation mechanisms. (B) Electromagnetic shielding performance of multilayer CNFaEUGb composite films.

mechanism of CNFaEUGb is proposed in Figure 6A. The establishment of the multilayer structure can trap and attenuate the entered electromagnetic waves by multiple reflection and interface scattering. As waves continue to propagate within the CNFaEUGb, the incident waves can be reflected repeatedly between two CNFs, thereby producing constructive interference and frequency-selective characteristics.

The structural characteristics and performance of typical EMI shielding materials (mainly multilayer carbon-based materials) are summarized in Table 2. Our CNFaEUGb composite films were prepared through simple infiltration and hot-pressing technologies, exhibiting comprehensive advantages, including flexibility, ultrathin thickness, high tensile strength, and excellent electromagnetic shielding performance. Moreover, due to the introduction of partially cross-linked EUG, CNFaEUGb possesses excellent shape memory ability and can respond quickly to infrared light, which will be discussed in the following section.

3.3. Shape Memory Behavior. Previous studies have revealed that thermal-triggered EUG-based shape memory materials can be obtained by the synthesis of partially cross-linked EUG.[17−22] However, it is inconvenient to achieve shape recovery by direct heating and may be limited by the application environment temperature in many fields. Infrared-triggered shape memory materials can make up for the shortcomings of traditional thermal SMPs.

In this work, CNFaEUGb was prepared with the combination of CNF and partially cross-linked EUG, and the infrared-responsive shape memory properties were characterized. The Control samples were prepared from EUG and 2% DCP through the hot-pressing process at a temperature of 150 °C and a pressure of 1 MPa for 30 min. As-prepared CNF5EUG5 are folded twice along the diagonal at 60 °C and quickly cooled to room temperature to fix their temporary shape and then exposed to infrared light (250 W bulb, Philips, testing distance of 20 cm) to observe their shape recovery behaviors (Figure 7A).

Table 2. Comparison of the Overall Performance of the Relevant Composites

samples	thickness (mm)	tensile stress (MPa)	SE (dB)	flexibility	ref
CNF3EUG5	0.08	108.5	70	√	our work
CNF5EUG5	0.18	92.6	88	√	our work
CNTs/GNPs/EUG	2.0	20.9	42.5	√	12
CNT-6−1100	6.0		25	×	13
CNT/UHMWPE	1.0	216.1	33.5	√	25
MWCNT/WPU	0.8		88	√	26
PMMA/rGO	2.9		63.2		27
SC-Co-G-0.9	2.0		55		29
CNF mats	2.9−5.4		52−81	√	31
GN-D-GN			17−49		33
PPC−PVAG-PPC		26.5	−24.49		34
PPC−PVAC-PPC		29.4	−36.70		34
PCS-WWW	2.0	66.7	−50		35
SG7.29-IG0T1.3	2.0		20.73−36.01	√	36
SBP-B	11.0		103	×	38
SCF/Epoxy	4.75		>70		39

Figure 7B,C display the infrared-triggered shape memory behaviors of the Control and CNF5EUG5 samples when exposed to the same intensity of infrared light. CNF5EUG5 exhibits a quick response and can recover to the permanent shape in 150 s. In contrast, the Control sample has a much slower response and cannot return to the permanent shape even after 10 min of infrared light exposure.

For the Control and CNF5EUG5 samples, the crystalline zones of EUG act as the reversible phase, and the cross-linking networks act as the fixed phase. The Control and CNF5EUG5 samples can be edited to a desired shape through heating at 60 °C and then cooling to RT and restoring its permanent shape by reheating to 60 °C. The mechanism of shape memory behavior is shown in Figure 7A. The EUG crystals melt when the temperature reaches 60 °C; thus, it is easy to be edited into the desired shape, the so-called temporary shape. When the temperature decreases to RT, EUG molecules gradually crystallize again to fix the temporary shape. As a photothermal conversion medium, CNF can effectively absorb infrared light and convert it into heat. Thus, CNF5EUG5 exhibited a quicker infrared response than the Control under the same infrared exposure conditions.

In addition, the influence of shape recovery cycles on the electromagnetic shielding performance is shown in Figure 8. After 20 and 40 recovery cycles, the appearance of CNF5EUG5 does not change significantly and the curves of SE_T values exhibit similar trends. However, some peak positions of the curves shift, and the peak values get a little lower. These results indicated that multiple cycle experiments have minor effects on the frequency-selective characteristics, which may come from the destruction of the interlayer

https://doi.org/10.1021/acsomega.4c07453
ACS Omega 2024, 9, 48563−48570

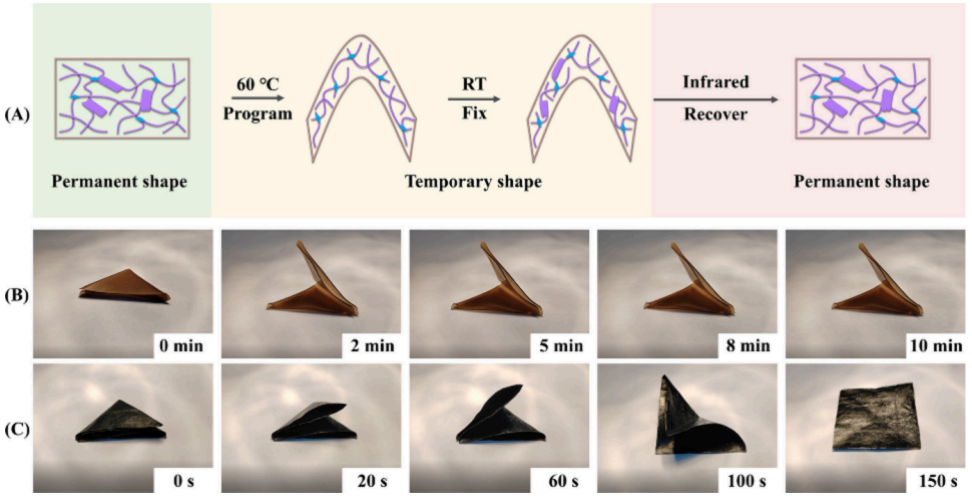

Figure 7. (A) Schematic representation of the infrared-triggered shape memory behaviors. Infrared-triggered shape memory recovery process of (B) the Control sample and (C) the CNF5EUG5 sample.

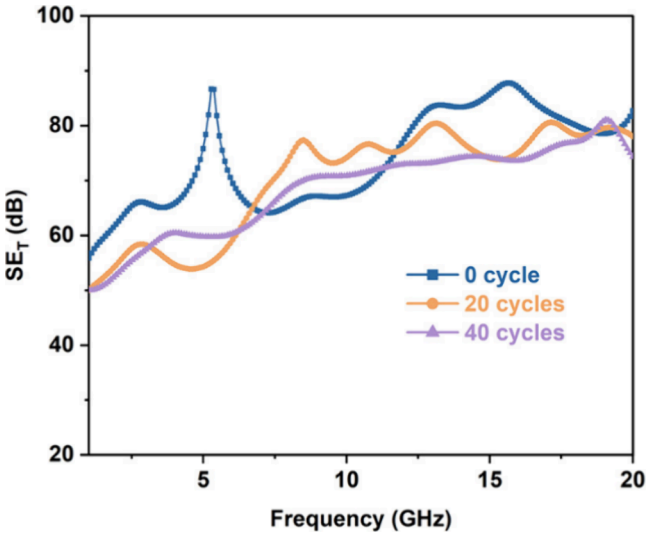

Figure 8. Electromagnetic shielding performance of CNF5EUG5 after 0, 20, and 40 recovery cycles.

structure during the shape fixation and recovery cycles. Nevertheless, the CNFaEUGb composite films have good infrared-triggered shape memory ability and can maintain excellent electromagnetic shielding performance after many shape fixation and recovery cycles.

4. CONCLUSIONS

In this work, multilayer CNF/EUG composite films with excellent mechanical and electromagnetic shielding performance and infrared-triggered shape memory ability have been fabricated successfully via infiltration and hot-pressing technologies. The number of CNF layers and infiltration cycles of the EUG solution have a crucial influence on the mechanical and electromagnetic shielding performance of composite films. The introduction of CNF can enhance the mechanical and electromagnetic shielding performance of multilayer CNF/EUG composite films. Partially cross-linked EUG can improve the elongation-at-break and endow composite films with shape memory behavior. The composite film CNF3EUG5 with a thickness of 80 μm has a maximum tensile stress of 108.4 MPa and a high SE_T value of 70 dB. As the CNF layer numbers increase, CNF5EUG5 with a thickness of 181 μm achieves the highest SE_T value of 88 dB but exhibits a lower tensile strength of 92.6 MPa. Attributed to the high photothermal conversion efficiency, CNF5EUG5 displays good shape memory capability when exposed to infrared light. These CNF/EUG composite films have great potential applications as electromagnetic shielding and infrared-triggered shape memory biomaterials.

AUTHOR INFORMATION

Corresponding Author

Bo-xing Zhang − *South China Advanced Institute for Soft Matter Science and Technology, School of Emergent Soft Matter and Guangdong Provincial Key Laboratory of Functional and Intelligent Hybrid Materials and Devices, South China University of Technology, Guangzhou 510640, China*; orcid.org/0000-0002-3399-5548; Email: bxzhang@scut.edu.cn

Author

Zhonglei Kang − *South China Advanced Institute for Soft Matter Science and Technology, School of Emergent Soft Matter, South China University of Technology, Guangzhou 510640, China*

Complete contact information is available at: https://pubs.acs.org/10.1021/acsomega.4c07453

Notes

The authors declare no competing financial interest.

ACKNOWLEDGMENTS

This work was financially supported by the Major Program of the National Natural Science Foundation of China (No. 51890871) and the Recruitment Program of Guangdong (No. 2016ZT06C322).

REFERENCES

(1) Wang, Q.; Xiong, Y.; Dong, F. *Eucommia Ulmoides* Gum-Based Engineering Materials: Fascinating Platforms for Advanced Applications. *J. Mater. Sci.* **2021**, *56* (2), 1855−1878.

(2) Wei, X.; Peng, P.; Peng, F.; Dong, J. Natural Polymer *Eucommia Ulmoides* Rubber: A Novel Material. *J. Agric. Food Chem.* **2021**, *69* (13), 3797−3821.

(3) Zhang, B.; Azuma, J.; Takeno, S.; Suzuki, N.; Nakazawa, Y.; Uyama, H. Improvement of the Rheological Properties of Trans-1,4-Polyisoprene from *Eucommia Ulmoides* Oliver by Tri-Branched Poly (Ricinoleic Acid). *Polym. J.* **2016**, *48* (7), 821−827.
(4) Yue, P.-P.; Leng, Z.-J.; Bian, J.; Li, M.-F.; Peng, F.; Sun, R.-C. Fast and Simple Construction of Composite Films with Renewable *Eucommia Ulmoides* Gum and Poly(ε-Caprolactone). *Compos. Sci. Technol.* **2019**, *179*, 145−151.
(5) Li, C.; Su, S.; Wang, B.; Zhou, J. Effects of *Eucommia* Gum Filler on the Dielectric Properties and Chemical Resistances of Addition-Cure Liquid Silicone Rubber. *J. Mater. Sci: - Mater. Electron.* **2021**, *32* (15), 20548−20558.
(6) Sarina; Zhang, J.; Zhang, L. Dynamic Mechanical Properties of *Eucommia Ulmoides* Gum with Different Degree of Cross-Linking. *Polym. Bull.* **2012**, *68* (7), 2021−2032.
(7) Ni, Q.; Wu, J.; Kong, P.; Wang, Y.; Li, Y.; Li, Y.; Peng, X. Inverse Vulcanization Polymer-Modified *Eucommia Ulmoides* Gum with Enhanced Shape Memory Capability and Sound Absorption Property. *ACS Appl. Polym. Mater.* **2022**, *4* (7), 4689−4698.
(8) Qi, X.; Zhao, X.; Li, Y.; Zhang, J.; Zhang, L.; Yue, D. A High Toughness Elastomer Based on Natural *Eucommia Ulmoides* Gum. *J. Appl. Polym. Sci.* **2021**, *138* (11), No. 50007.
(9) Qi, X.; Xie, F.; Zhang, J.; Zhang, L.; Yue, D. Bio-Based Cyclized *Eucommia Ulmoides* Gum Elastomer for Promising Damping Applications. *RSC Adv.* **2019**, *9* (72), 42367−42374.
(10) Chen, B.; Wu, Q.; Li, J.; Lin, K.; Chen, D.; Zhou, C.; Wu, T.; Luo, X.; Liu, Y. A Novel and Green Method to Synthesize a Epoxidized Biomass Eucommia Gum as the Nanofiller in the Epoxy Composite Coating with Excellent Anticorrosive Performance. *Chem. Eng. J.* **2020**, *379*, No. 122323.
(11) Yang, H.; Peng, P.; Sun, Q.; Zhang, Q.; Ren, N.; Han, F.; She, D. Developed Carbon Nanotubes/Gutta Percha Nanocomposite Films with High Stretchability and Photo-Thermal Conversion Efficiency. *J. Mater. Res. Technol.* **2020**, *9* (4), 8884−8895.
(12) Kang, H.; Luo, S.; Du, H.; Han, L.; Li, D.; Li, L.; Fang, Q. Bio-Based Eucommia Ulmoides Gum Composites with High Electromagnetic Interference Shielding Performance. *Polymers* **2022**, *14* (5), 970.
(13) Kang, Z.; Hu, H.; Uyama, H.; Zhang, B. Porous Eucommia Ulmoides Gum Monoliths Prepared via Modified Pickering High Internal Phase Emulsion Method. *ACS Appl. Polym. Mater.* **2023**, *5* (8), 6117−6123.
(14) Wang, E.; Wu, Y.; Islam, Md. Z.; Dong, Y.; Zhu, Y.; Liu, F.; Fu, Y.; Xu, Z.; Hu, N. A Novel Reduced Graphene Oxide/Epoxy Sandwich Structure Composite Film with Thermo-, Electro- and Light-Responsive Shape Memory Effect. *Mater. Lett.* **2019**, *238*, 54−57.
(15) Lu, H.; Li, Z.; Qi, X.; Xu, L.; Chi, Z.; Duan, D.; Islam, M. Z.; Wang, W.; Jin, X.; Zhu, Y.; Fu, Y.; Cui, L.; Zhuang, Y.; Dong, Y. Flexible, Electrothermal-Driven Controllable Carbon Fiber/Poly (Ethylene-Co-Vinyl Acetate) Shape Memory Composites for Electromagnetic Shielding. *Compos. Sci. Technol.* **2021**, *207*, No. 108697.
(16) Ozdemir, V. B.; Kwok, K. Electro-Thermo-Mechanical Behavior of Carbon Nanopaper Shape Memory Polymer Composites. *J. Intell. Mater. Syst. Struct.* **2022**, *33* (3), 489−500.
(17) Qi, X.; Xu, E.; Jia, M.; Zhang, J.; Zhang, L.; Yue, D. Bio-Based, Self-Crosslinkable *Eucommia Ulmoides* Gum/Silica Hybrids with Body Temperature Triggering Shape Memory Capability. *Macromol. Mater. Eng.* **2021**, *306* (11), No. 2100370.
(18) Tsujimoto, T.; Toshimitsu, K.; Uyama, H.; Takeno, S.; Nakazawa, Y. Maleated Trans −1,4-Polyisoprene from Eucommia Ulmoides Oliver with Dynamic Network Structure and Its Shape Memory Property. *Polymer* **2014**, *55* (25), 6488−6493.
(19) Wang, Y.; Liu, J.; Xia, L.; Shen, M.; Xin, Z. Super-Tough Poly (Lactic Acid) Thermoplastic Vulcanizates with Heat Triggered Shape Memory Behaviors Based on Modified Natural Eucommia Ulmoides Gum. *Polym. Test.* **2019**, *80*, No. 106077.
(20) Xia, L.; Chen, S.; Fu, W.; Qiu, G. Shape Memory Behavior of Natural *Eucommia Ulmoides* Gum and Low-Density Polyethylene Blends with Two Response Temperatures. *Polymers* **2019**, *11* (4), 580.
(21) Xia, L.; Yang, F.; Wu, H.; Zhang, M.; Huang, Z.; Qiu, G.; Xin, Z.; Fu, W. Novel Series of Thermal- and Water-Induced Shape Memory *Eucommia Ulmoides* Rubber Composites. *Polym. Test.* **2020**, *81*, No. 106212.
(22) Qi, X.; Zhang, J.; Zhang, L.; Yue, D. Bio-Based, Robust, Shape Memory, Self-Healing and Recyclable Elastomers Based on a Semi-Interpenetrating Dynamic Network. *J. Mater. Chem. A* **2021**, *9* (45), 25399−25407.
(23) Xia, L.; Wang, Q.; Meng, J.; Ma, Z.; Zhao, P. Thermal and Electro-induced Shape-memory *Eucommia Ulmoides* Gum Composites Filled with Carbon Nanotubes. *Polym. Adv. Technol.* **2021**, *32* (8), 3297−3308.
(24) Xia, L.; Liu, X.; Wang, Q.; Ma, Z.; Huang, Z. Study of Electro-Induced Shape-Memory *Eucommia Ulmoides* Rubber Composites Reinforced with Conductive Carbon Blacks. *Express Polym. Lett.* **2021**, *15* (7), 600−611.
(25) Yu, W.-C.; Zhang, G.-Q.; Liu, Y.-H.; Xu, L.; Yan, D.-X.; Huang, H.-D.; Tang, J.-H.; Xu, J.-Z.; Li, Z.-M. Selective Electromagnetic Interference Shielding Performance and Superior Mechanical Strength of Conductive Polymer Composites with Oriented Segregated Conductive Networks. *Chem. Eng. J.* **2019**, *373*, 556−564.
(26) Zeng, Z.; Chen, M.; Jin, H.; Li, W.; Xue, X.; Zhou, L.; Pei, Y.; Zhang, H.; Zhang, Z. Thin and Flexible Multi-Walled Carbon Nanotube/Waterborne Polyurethane Composites with High-Performance Electromagnetic Interference Shielding. *Carbon* **2016**, *96*, 768−777.
(27) Sharif, F.; Arjmand, M.; Moud, A. A.; Sundararaj, U.; Roberts, E. P. L. Segregated Hybrid Poly (Methyl Methacrylate)/Graphene/Magnetite Nanocomposites for Electromagnetic Interference Shielding. *ACS Appl. Mater. Interfaces* **2017**, *9* (16), 14171−14179.
(28) Li, H.; Liu, L.; Li, H.-B.; Song, W.-L.; Bian, X.-M.; Zhao, Q.-L.; Chen, M.; Yuan, X.; Chen, H.; Fang, D. Assembling Carbon Fiber−Graphene−Carbon Fiber Hetero-Structures into 1D−2D−1D Junction Fillers and Patterned Structures for Improved Microwave Absorption. *J. Phys. D: Appl. Phys.* **2017**, *50* (13), 135303.
(29) Xu, Z.; Liang, M.; He, X.; Long, Q.; Yu, J.; Xie, K.; Liao, L. The Preparation of Carbonized Silk Cocoon-Co-Graphene Composite and Its Enhanced Electromagnetic Interference Shielding Performance. *Composites Part A* **2019**, *119*, 111−118.
(30) Wang, L.; Ma, Z.; Zhang, Y.; Chen, L.; Cao, D.; Gu, J. Polymer-Based EMI Shielding Composites with 3D Conductive Networks: A Mini-Review. *SusMater.* **2021**, *1* (3), 413−431.
(31) Hong, X.; Chung, D. Carbon Nanofiber Mats for Electromagnetic Interference Shielding. *Carbon* **2017**, *111*, 529−537.
(32) Zhang, C.; Li, Y.; Kang, W.; Liu, X.; Wang, Q. Current Advances and Future Perspectives of Additive Manufacturing for Functional Polymeric Materials and Devices. *SusMater.* **2021**, *1* (1), 127−147.
(33) Song, W.-L.; Gong, C.; Li, H.; Cheng, X.-D.; Chen, M.; Yuan, X.; Chen, H.; Yang, Y.; Fang, D. Graphene-Based Sandwich Structures for Frequency Selectable Electromagnetic Shielding. *ACS Appl. Mater. Interfaces* **2017**, *9* (41), 36119−36129.
(34) Lin, J.-H.; Lin, Z.-I.; Pan, Y.-J.; Huang, C.-L.; Chen, C.-K.; Lou, C.-W. Polymer Composites Made of Multi-Walled Carbon Nanotubes and Graphene Nano-Sheets: Effects of Sandwich Structures on Their Electromagnetic Interference Shielding Effectiveness. *Composites Part B* **2016**, *89*, 424−431.
(35) Lai, M.-F.; Huang, C.-H.; Lin, J.-H.; Chuang, Y.-C.; Wang, C.-H.; Lou, C.-W. Polypropylene/Carbon Fiber Composite Layered Materials: Electromagnetic Interference Shielding Effect and Mechanical Performance. *Fiber. Polym.* **2021**, *22* (9), 2552−2562.
(36) Wang, G.; Liao, X.; Yang, J.; Tang, W.; Zhang, Y.; Jiang, Q.; Li, G. Frequency-Selective and Tunable Electromagnetic Shielding Effectiveness via the Sandwich Structure of Silicone Rubber/Graphene Composite. *Compos. Sci. Technol.* **2019**, *184*, No. 107847.
(37) Sun, H.; Shi, G.; Kang, Z.; Zhong, H.; Han, W.; Luo, Z.; Zhang, B. Thin and Flexible Multilayer Carbon/Silicon Carbide Composite

https://doi.org/10.1021/acsomega.4c07453
ACS Omega 2024, 9, 48563−48570

Films with Extraordinary Electromagnetic Shielding Performance and Ablative Resistance. *Carbon* **2024**, *230*, No. 119660.
(38) Hu, Y.; Li, D.; Wu, L.; Yang, J.; Jian, X.; Bin, Y. Carbon Nanotube Buckypaper and Buckypaper/Polypropylene Composites for High Shielding Effectiveness and Absorption-Dominated Shielding Material. *Compos. Sci. Technol.* **2019**, *181*, No. 107699.
(39) Liang, J.; Bai, M.; Gu, Y.; Wang, S.; Li, M.; Zhang, Z. Enhanced Electromagnetic Shielding Property and Anisotropic Shielding Behavior of Corrugated Carbon Fiber Felt Composite and Its Sandwich Structure. *Composites Part A* **2021**, *149*, No. 106481.
(40) Zhou, Z.; Song, Q.; Huang, B.; Feng, S.; Lu, C. Facile Fabrication of Densely Packed Ti_3C_2 MXene/Nanocellulose Composite Films for Enhancing Electromagnetic Interference Shielding and Electro-/Photothermal Performance. *ACS Nano* **2021**, *15* (7), 12405−12417.
(41) Shen, B.; Li, Y.; Zhai, W.; Zheng, W. Compressible Graphene-Coated Polymer Foams with Ultralow Density for Adjustable Electromagnetic Interference (EMI) Shielding. *ACS Appl. Mater. Interfaces* **2016**, *8* (12), 8050−8057.
(42) Jiang, X.; Yu, H.; Lu, H.; Si, Y.; Dong, Y.; Zhu, Y.; Qian, C.; Fu, Y. Anisotropic Shape Memory Composite for Dynamically Adjustable Electromagnetic Interference Shielding. *ACS Appl. Mater. Interfaces* **2023**, *5* (6), 4400−4410.
(43) He, Y.; Shao, Y.; Xiao, Y.; Yang, J.; Qi, X.; Wang, Y. Multifunctional Phase Change Composites Based on Elastic MXene/Silver Nanowire Sponges for Excellent Thermal/Solar/Electric Energy Storage, Shape Memory, and Adjustable Electromagnetic Interference Shielding Functions. *ACS Appl. Mater. Interfaces* **2022**, *14* (4), 6057−6070.
(44) Song, Q.; Ye, F.; Yin, X.; Li, W.; Li, H.; Liu, Y.; Li, K.; Xie, K.; Li, X.; Fu, Q.; Cheng, L.; Zhang, L.; Wei, B. Carbon Nanotube−Multilayered Graphene Edge Plane Core−Shell Hybrid Foams for Ultrahigh-Performance Electromagnetic-Interference Shielding. *Adv. Mater.* **2017**, *29* (31), No. 1701583.

https://doi.org/10.1021/acsomega.4c07453
ACS Omega 2024, 9, 48563−48570